US-FT 94-1
US-FT/1-94 Su 9409

Monte Carlo Model for Multiparticle Production at Ultra-Relativistic Energies

N. S. Amelin[1], H. Stöcker and W. Greiner
Institut für Theoretische Physik, Universität Frankfurt,
Postfach 111932, D-6054 Frankfurt am Main 11, Germany

N. Armesto, M. A. Braun[2] and C. Pajares
Departamento de Física de Partículas, Universidade de Santiago de Compostela,
15706-Santiago de Compostela, Spain

Abstract

The Monte Carlo Parton String Model for multiparticle production in hadron-hadron, hadron-nucleus and nucleus-nucleus collisions at high energies is described. In this model inelastic hadron or nuclear interactions are reduced to interactions between partons. An adequate choice of the parton parameters gives the possibility of recovering main results of the Dual Parton Model. Both soft and hard parton interactions are considered, leading to the excitation of longitudinal and kinky strings respectively. By comparing the predicted quantities to the available experimental data, the applicability of the model in nucleon and nuclear collisions is shown. Predictions for mean multiplicities, central rapidity densities of light flavour and charmed hadrons, net baryon rapidity distributions and the temporal evolution of the meson density are presented for massive ion collisions at CERN-$Sp\bar{p}S$ (19.4 $AGeV$) and BNL-$RHIC$ (200 $AGeV$).

US-FT/1-94
February 1994

---

[1]Alexander von Humboldt Research Fellow; on leave of absence from the JINR, Dubna, Russia.

[2]On leave of absence from St. Petersburg University, Russia.

1 Introduction

The search of the Quark–Gluon Plasma (QGP) is the goal of the experimental heavy–ion program ([1]). Nevertheless, almost all the data coming from Brookhaven (AGS) and CERN ($Sp\bar{p}S$) can be described by models ([2, 3, 4, 5, 6]) based on the production of colour strings, which decay independently into the observed hadrons.

The existing data are limited to relatively light ions and energies in the range $E_{lab} = 10 - 200$ $AGeV$. It is planned to study the heaviest nucleus collisions, when massive ion beams are available up to collider energies: $E_{cm} = 100$ $AGeV$ at Brookhaven ($RHIC$) and $E_{cm} = 3000$ $AGeV$ at CERN (LHC). Collisions of massive ions are expected to lead to the creation of extremely dense hadronic matter. A change in the hadron production mechanism is also expected: at lower energies hadrons are produced essentially in soft collisions with small transferred momenta; at collider energies the so called semi–hard processes ([9]) will dominate. The momenta transferred in such collisions are large enough to use Perturbative Quantum Chromodynamics (PQCD) calculations.

All the succesfull string models for nuclear collisions are essentially hadron based models, in which nuclear interactions are reduced to hadron interactions. The models in Refs. [3, 6] are hadron cascade models, in which the interaction with the nuclear target is reduced to successive interactions with separate nucleons. For the validity of the cascade approach the density of the hadronic matter should be low, so that two consecutive scatterings can be distinguished at the hadronic level. These models give the possibility to consider evolution of the colliding system, although predictions are limited, since they can only operate with a size scale larger than the hadronic size. Other models ([2, 4, 5]) do not consider evolution, and treat nuclear interactions as "simultaneous" interactions in the impact parameter plane. These models are based on the Glauber approach, in which energy independent inelastic hadron–nucleon cross sections are used to find the probability of several hadron interactions. For both kind of models, quark and gluon degrees of freedom are used to compute the string formation parameters.

In this paper the Monte Carlo Parton String Model predictions for multiparticle production in hadronic collisions at $E_{cm} = 19.4$, 200 and 1800 GeV are presented. The first description of this numerical model can be found in Ref. [8], where the influence of string interaction on multiple production was studied. This approach is based on the parton picture of strong interactions, and also on its properties following from the Regge formalism ([10]), in which hadron and nucleus collisions are reduced to interactions of partons, with given distributions in the projectile and target. We distinguish "soft" and "hard" parton interactions. Soft parton collisions, when the transferred momenta are neglected, lead to the creation of longitudinal strings. Additionally, we introduce hard perturbative parton–parton collisions and parton bremsstrahlung, whose inclusion leads to the creation of kinky strings.

2 Model description

2.1 Parton collision probability: string formation

At high energy, a fast moving hadron or nucleus can be considered as a superposition of parton (mostly gluon) chains or cascades. A hadron or nucleus collision is assumed to be the interaction between slow partons (chain or cascade tails) from the projectile and target. The distribution in the number of interacting partons is directly connected with the values of the multipomeron vertices in the reggeon theory ([10]). In the eikonal approximation it takes a Poissonian form:

$$w_N^{(1)} = \exp(-g(s))g^N(s)/N! \ . \qquad (1)$$

The mean number of the strongly interacting partons, $g(s) = g_0 s^{\Delta}$, is a function of the initial energy $\sqrt{s}$. We use $g_0 = 3.0$ and $\Delta = 0.09$. The parton–parton cross section has been assumed energy independent, $\sigma_p = 3.5\ mb$. Each parton is allowed to interact only once, to exclude the contribution of planar diagrams, which dies out at high energies.

In accordance with the Pomeron picture of strong interactions, the slow parton distribution in impact parameter (relative to the center of the corresponding hadron) is taken to be Gaussian:

$$F(b_p) = (4\pi\lambda)^{-1}\exp(-b_p^2/4\lambda), \qquad (2)$$

with the radius depending on the initial hadron energy. For a projectile or target nucleon, $\lambda = R^2 + \alpha' \ln\sqrt{s}$, where $\alpha' = 0.01\ fm^2$ and $R^2 = 0.15\ fm^2$.

Parton–parton interactions destroy the coherence of the parton chains, which leads to hadronization. As in the standard Dual Parton Model (DPM, [11, 12]), where each cut Pomeron is substituted by two strings, we assume that hadronization goes through the decay of strings. Each inelastic parton–parton collision creates two colour strings. The momenta $p_{\pm}$ of the partons at the ends of the strings are given by the nucleon structure functions in $x_{\pm} = p_{\pm}/P_{\pm}$, where $P_{\pm}$ is the momentum of the nucleon to which they belong. The nucleon structure function is assumed factorized, except for energy–momentum conservation:

$$u(x_1, x_2, ..., x_n) = \delta(1 - \sum_{i=1}^{n} x_i)\prod_{i=1}^{n} u_i(x_i). \qquad (3)$$

For the single parton distributions $u_i(x)$, the ones obtained from the Regge theory are used ([12]):

$$u_v(x) = u_s(x) = x^{-0.5},\ u_{vv}(x) = x^{1.5} \ , \qquad (4)$$

except for strange sea quarks, for which $u_s(x) = 1/x$, with a cutoff in x ($x > x_{min} = m_t/P_+$), is used. v, s and vv refer to valence and sea quarks and diquarks respectively. We use a strangeness suppression parameter $\gamma_s^h = 0.3$, as in the string decay (see below), to find a strange sea quark pair inside the nucleon. According to Eq. (2), a Gaussian form is also taken for the p_t distribution of partons sitting on the string ends:

$$f(p_t^2)p_t dp_t \sim \exp(-bp_t^2)p_t dp_t \ , \tag{5}$$

with $b = 4\ GeV^{-2}$.

The quality of the choice of the parton distributions and the cross section σ_p is demonstrated in Fig. 1, where the inelastic NN cross sections are compared to experimental data. Fig. 2 shows the dependence of the average number of parton collisions $< N^p_{coll} >$ on the impact parameter b, in pp interactions at $Sp\bar{p}S$, $RHIC$ and LHC energies. In central collisions (here and further on, a central collision means $b = 0$), this value changes from 2 at 19.4 GeV to 8 at 6300 GeV.

For nuclear collisions, the parton distributions for individual nucleons are taken to be the same as for NN collisions. The final nuclear parton wave function is the convolution of these parton distributions, with the distribution of nucleons inside the nucleus. For the latter we use the Woods–Saxon density:

$$\rho(r) \ = \rho_0/(1 + \exp[(r - r_0)/a]), \tag{6}$$

with

$$r_0 = 1.19A^{1/3} + 1.61A^{-1/3}\ fm,\ a \ = \ 0.54\ fm. \tag{7}$$

The distribution in the number of interacting nucleons from the projectile nucleus is presented in Fig. 3, for ^{16}OAu collisions at 200 $AGeV$, in comparison with the predictions of the VENUS model ([4]). They look quite similar. The distribution in the number of interacting partons is also shown in this figure.

The Fermi motion of nucleons is also taken into account. A Fermi momentum p is uniformly generated for each nucleon, in the range $0 < p < p_F$, where p_F is the maximum Fermi nucleon momentum:

$$p_F = (3\pi^2)^{1/3} h \rho^{1/3}(r), \tag{8}$$

where $h = 0.197\ fmGeV/c$. To determine the nucleon coordinates and momenta, an isotropical angular distribution is assumed.

2.2 String decay

The approaches most commonly used to simulate the string decay are: the Artru–Mennessier model ([13]), the Field–Feynman algorithm ([14]), and the most popular one, the Lund fragmentation model ([30]). All of them treat string decay through the creation of quark–antiquark or diquark–antidiquark pairs with transverse masses. In all models, the parameters are extracted from the comparison to e^+e^- and lN data. In this sense, they give equal results for hadron collisions.

In our case, the modelling of the decay of a string with a given mass, momentum and quark content, is carried out by the Field–Feynman algorithm ([14]). At each string break–up the strangeness suppression parameter is $\gamma_s = 0.3$ and the ratio of the diquark–antidiquark pair production to the quark–antiquark one has been set equal to: $P_{qq,\overline{qq}} : P_{q\bar{q}} = \gamma_{B\bar{B}} = 0.09$. Equal probabilities of producing pseudoscalar and vector mesons from quarks and antiquarks, and baryons with spin 1/2 and 3/2 from quarks and diquarks, are assumed. At a string break–up the $q\bar{q}$ pair has zero total transverse momentum, the momenta of the quark $\vec{p}_t$ and the corresponding antiquark $-\vec{p}_t$ being distributed according to Eq. (5), with $b = 8.2\ (GeV/c)^{-2}$. For a produced hadron, its transverse momentum consists of the transverse momenta of its quarks, and the longitudinal momentum p_z^h and energy E^h are determined through the variable $z = (E^h + p_z^h)/(E^q + p_z^q)$ (E^q energy and p_z^q longitudinal momentum of the fragmenting quark), following the distribution:

$$f_h^q(z) \sim (1-z)^{\alpha_q^h(p_t)} \quad . \tag{9}$$

At $z \to 1$, this function coincides with the fragmentation function $D_q^h(z)$ of the leading quark (antiquark) or diquark (antidiquark) into a hadron. $\alpha_q^h(p_t)$ depends ([12]) on the flavour of the constituent quark, and on the type of hadron it is transformed into and its transverse momentum. The requirement that the fragmentation function $D_q^h(z) \to 1/z$, for $z \to 0$, is ensured by iterating string break–ups. If the mass of a string, M_s, is less than $M_c = M_R + \Delta M$, where $\Delta M = 0.35\ GeV$ and M_R is the mass of the resonance with the same quark composition as the string, the last break is generated. Its kinematics is determined by the isotropy of the emission of two hadrons. The newly produced resonances are assumed unpolarized, and hence, they decay isotropically, for which the experimentally known branching ratios are used.

3 Comparison to experimental data

3.1 The data at $E_{cm} = 19.4\ AGeV$

In Fig. 4 and Fig. 5, the model results at $E_{cm} = 19.4\ AGeV$ (CERN–$Sp\bar{p}S$) in proton–proton, proton–nucleus and nucleus–nucleus collisions are shown, together with experimental data. As one can see from Fig. 4, the model reproduces successfully the experimental rapidity and multiplicity distributions for negative particles. It also describes satisfactorily the strange hadron production in pp and pA collisions ([8]), except the shape of the rapidity distribution of Λ's measured by the NA35 Collaboration ([7]). However, the model does not predict any low p_t enhancement, which is visible in the NA35 experiment for central SS collisions, and more pronounced for heavier colliding systems ([16]). As it was demonstrated earlier ([8]), our model fails to reproduce the mean number of strange baryons and their rapidity distributions in central SS collisions (without additional mechanisms).

The proton transverse momentum distributions in nuclear collisions are very sensitive to the chosen primordial quark momenta and can be fitted by changing some parameters. Since nuclear cascading of secondaries is not taken into account, our model is not able to reproduce positive particle (proton) rapidity distributions in the nucleus fragmentation region. It is known ([3, 6]) that secondary cascading can improve the description of the proton rapidity distributions, and also changes essentially transverse momentum distributions, particularly, the low momentum pion distribution, as a result of creation and decay of Δ resonances. It can enhance the strangeness production on nuclear targets due to resonance–nucleon interactions.

3.2 Charm production

As it was shown in Refs. [17, 18], the analytical Quark–Gluon String Model (QGSM, [12]) gives a reasonable description of the existing data on charm production: it reproduces satisfactorily the cross sections and the spectra of charmed particles produced in nucleon and nuclear collisions. Usually heavy flavour production processes are considered in the framework of PQCD, but these calculations are very sensitive to many factors, particularly to the low x extrapolation of the gluon structure function. Predictions of QGSM and PQCD (with absorptive corrections taken into account) are shown to coincide through a large energy range ([18]).

In our Monte Carlo approach the fragmentation functions shown in Eq. (9), taken from Ref. [12], are used. The exponent $\alpha_q^h(p_t)$ is defined by the quantity α_ψ – the intercept of the Regge trajectory for the ψ family, not well known. Our choice is $\alpha_\psi = -2.2$. A suppression parameter for charmed quark pairs, as for strange quark pairs, is used: from comparison to the experimental data ([19]), $\gamma_{c\bar{c}} = 0.0025$. Cross sections for different charmed particles are compared with the experimental data in Table 1, for 100000 simulated events. This statistics is too small to extract x distributions for different particles, but enough to show the prediction of the model for all D–mesons (Fig. 6).

3.3 The data at $E_{cm} = 200\ AGeV$

In Table 2 we compare the mean numbers of produced particles to the experimental data. The production of strange particles and anti–baryons is fully determined by the fragmentation parameters: the strangeness and baryon–antibaryon suppression factors described above. In Fig. 7, some experimental data are plotted together with the model predictions. With the exception of the low multiplicity event underestimation, the model reproduces well the experimental data. The reason for this discrepancy might be connected with the fragmentation procedure, or with the neccesity of including some additional mechanism, like diffraction.

4 Inclusion of hard parton scattering

So far, only soft interactions between partons have been considered: no momentum, only colour charge, can be transferred during each parton collision. The picture of the interaction is an even number of longitudinal colour strings, spanned between colour triplet quarks or diquarks, moving into opposite directions in the string rest frame. The necessity of the inclusion of hard parton scattering is demonstrated in Fig. 8. At $E_{cm} = 200\ GeV$, the model is not able to describe the transverse momentum distribution in the whole p_t region, the agreement exists only for $p_t \leq 1.5 - 2\ GeV/c$.

In PQCD ([9]) a fast moving hadron can be considered as a superposition of parton (mostly gluon) chains or cascades, which have increasing transverse momenta along themselves. Small x partons of chains from the projectile will interact hard with small x partons from the target, if they are close in impact parameter. The final states obtained in hard processes can be described in term of strings spanned between the quarks, where gluons are treated as internal kink excitations on strings ([24]), so that hard perturbative processes will lead to kinky string states.

Up to now, a unified treatment of high energy hadronic collisions in the framework of QCD does not exist. There are different phenomenological approaches, which try to combine "soft" and "hard" parton interactions. In the Regge theory language, it means the combination of exchanges of "soft" and "hard" Pomerons. The most popular is the eikonal approach ([25, 26, 27, 28]), in which the probability to have a hard parton interaction (a "hard" cut Pomeron) is obtained from the jet production cross section, by using an eikonal unitarization procedure. Recently, the Lund approach ([2]) has been developed, in which a smooth transition from soft to hard parton interactions is provided by the so called soft gluon radiation. To simulate gluon radiation the Lund soft dipole model ([31]) implemented in the ARIADNE code is used. In hadron collisions hard gluons (kinks on strings) are point-like sources of the associated gluon radiation. Quarks or diquarks sitting at the ends of a string are considered as extended sources of gluon radiation, which leads to a suppression of the gluon radiation in the fragmentation regions of both ends. The momentum $p_{t,hard}$ transferred during hard gluon-gluon scatterings should be larger than any $p_{t,rad}$ momentum transferred during gluon radiation. This condition is used in the Lund approach ([2]) as an effective cut-off for hard parton scattering, i. e., hard parton-parton scatterings are accepted only if $p_{t,hard} > p_{t,rad}$.

By taking into account the soft and hard processes, we have two mechanisms for string excitation: through longitudinal quark motion, and through hard parton-parton scattering. In the case of a hard parton-parton scattering, a kinky string is produced, and the string energy-momentum is the sum of the energy-momenta of the hard scattered parton, and the longitudinaly moving quarks sitting on the string ends.

In our model, two different possibilities have been considered so far:

1. Each parton-parton collision is taken to be a hard one, and then gluon radiation is allowed. If the Lund criteria ($p_{t,hard} > p_{t,rad}$, as explained above) is not fulfilled, the collision is treated as a soft one.

2. We assume that each parton–parton collision can be a hard one, with the probability $w(s)$, which is a function of the initial hadron energy $\sqrt{s}$.

In the simulations presented in this section, the second alternative has been used. Only gluon–gluon ($gg \to gg$) hard scatterings are considered, using the PYTHIA program ([30]). Since the parton cross sections diverge for $p_t \to 0$, a cut-off $p_t^{min} = 2.3$ GeV/c is introduced. The EHLQ set 1 structure functions ([29]), inserted in the PYTHIA program as a default parameter, are used in these calculations. In the case of several n hard collisions for gluons belonging to the same hadron, the joint structure function should be used; here, each collision is considered independent, except for $\sum_{i=1}^{n} x_i \sim 1$. Some comparison to experimental data can be seen in Fig. 9. To calculate the distributions shown in this figure, we used $w(s) = 1 - \exp\left[-0.025(s - 376.4)^{0.03}\right]$. The associated gluon radiation was simulated by the ARIADNE code ([31]). The Lund string fragmentation model ([30, 32]) was applied to simulate the decay of the kinky strings. The default parameters of these programs were used during the simulations.

It follows from our calculations that it is possible to predict the shape of the pseudorapidity distributions and the increase of the central pseudorapidity density with energy for both versions of the model: the pure "soft" version, in which neither hard gluon scattering nor gluon radiation are included, and the "hard+soft" version, with both effects included. But only the latter gives reasonable predictions for p_t distributions.

5 Model predictions for massive ion beams

In this section, some predictions for massive ion collisions at energies $E_{cm} = 19.4$ $AGeV$ and $E_{cm} = 200$ $AGeV$ are presented. So far all calculations discussed below have been done without hard gluon scatterings and gluon radiation.

5.1 Light flavor and charmed particle production

Charged and negative particle rapidity distributions are shown in Fig. 10 for pp, pAu, $AuAu$ and central $AuAu$ collisions. The values of the maximum of the charged rapidity density are ~ 800 and ~ 1600 at $Sp\bar{p}S$ and $RHIC$ energies respectively for central $AuAu$ collisions. It is more or less close to existing calculations ([18]).

Negative particle multiplicity distributions are presented in Fig. 11 (integrated over the whole rapidity space). The production of about one thousand particles in central $AuAu$ collisions, as well as the narrowness of the central multiplicity distributions, point out the possibility to make an one-per-one event experimental analysis.

Some other event characteristics are presented in Tables 3. Our model did not take into account nucleon elastic scattering nor diffraction dissociation nor secondary rescatterings of the produced hadrons in the nuclear medium. Therefore the number of nucleons should be strongly underestimated. Two factors are essential to produce strange hadrons, baryon–antibaryon pairs and charmed hadrons: suppresion parameters for the string decay, and string masses. String masses depend on the structure functions, x cuts, initial energy and colliding system. In central $AuAu$ collisions, at $E_{cm} = 19.4\ AGeV$, the initial energy is shared among about one thousand strings. This leads to a kinematical suppression of heavy hadrons. The influence of this kinematical factor is much less at $RHIC$ energy, as can be seen in Tables 3. The model fails to reproduce the enhancement of strange baryons in central nucleus–nucleus collisions, observed in the NA35 experiment ([7]). For this reason, the predictions for strange baryon production in central massive ion collisions should be much lower than the experimental data.

As shown above, the model gives a reasonable agreement with the existing data on charm production in pp collision at $E_{cm} = 27.4\ GeV$. Production of charmed hadrons in ultra–relativistic massive ion collisions offers an opportunity to study different aspects of nuclear reactions, such as the thermalization time ([33]), multy–heavy charmed baryon production in the presence of QGP ([34]) etc. It seems to be quite instructive to give a prediction on charm production on nuclear targets, although good quantitative accuracy, especially for central $AuAu$ collisions, is not intended. At $E_{cm} = 200\ GeV$ the model predicts ~ 5 charmed particles in each central event, and the central rapidity density of charmed particles can reach one. This large amount of charmed particles can open interesting perspectives for the creation of high energy neutrino beams ([35]), particularly for the yet unobserved ν_τ.

It should be stressed that in our model, as in most string models, the produced strings do not interact and decay independently. Introduction of some collective effects, like string fusion ([8]), can change the predictions essentially, especially for rapidity plateau heights and high multiplicity distribution tails.

5.2 Nuclear stopping power

In Tables 3 predictions for the relative position of the maxima of the rapidity net proton distributions are presented to illustrate the so called nuclear stopping power. The rapidity shift is determined by how the total nucleon momentum is divided among partons sitting on the ends of the strings, i. e. by the quark and diquark structure functions and their number. In our case the number of partons increases with the initial energy. But the rapidity shift is weakly dependent on energy for a given parton number, since the structure function is a product of $x^{-0.5}$'s. With a different sea quark structure function, say $1/x$ as in the DPM ([11]), the rapidity shift decreases with energy, due to the introduced x–cut ([38]). The rapidity shift is also dependent on the fragmentation function of a diquark to produce a proton. As it follows from our calculations, the rapidity shift per soft parton–parton collision is approximately $\sim 0.40 - 0.45$. We want to stress that these distributions are obtained in the model with no secondary parton or hadron rescattering.

5.3 Meson density evolution

To have some information about the evolution of the colliding system we use the simple idea of Ref. [36]. In the Lund model ([37]) the time t_i and coordinate z_i of the hadron i, produced in the string decay, are defined by:

$$t_i = (1/2\kappa)[M_s - 2\sum_{j=1}^{i-1} p_{z_j}] + E_i - p_{z_i} \quad , \tag{10}$$

$$z_i = (1/2\kappa)[M_s - 2\sum_{j=1}^{i-1} E_j] + p_{z_i} - E_i \quad , \tag{11}$$

in the string center of mass. Here index $i = 1, 2, \ldots$ orders the string break–up points, M_s is the string mass, $\kappa \sim 1\ GeV/fm$ is the string tension, and p_{z_i} and E_i are the hadron longitudinal momentum and energy respectively. Quarks are assumed to be massless. To find the hadron time and coordinate in the observer frame Lorentz boosts and rotations are performed. If interactions of hadrons after their production through string decay are neglected, the time evolution of particle and energy density can be calculated, since the time, coordinates and momenta of the produced hadrons are known. The predictions are very limited by the absence of information about longitudinal coordinates and time of the string formation points. They are assumed to be equal zero. It is not a realistic assumption, because the low momentum initial partons, whose interaction leads to string formation, should be smeared in longitudinal length; however, it gives a possibility to clearly see a finite hadron production time, presented in Fig. 12 for mesons. In our model mesons are produced only after $0.5 - 1\ fm/c$. Since the hadron formation time in this Lund definition ([37]) is proportional to the transverse hadron mass, baryons are produced later than mesons, after $\sim 2\ fm/c$. It is a long time as compared with the temporal evolution extracted from models based on only hard parton scatterings. Particularly, at $RHIC$ energy in the hard parton collision model of Ref. [39] already after $2\ fm/c$ an equilibrated parton gas can be established.

To estimate local meson density as a function of time in the center of mass of the colliding nuclei we choose a box with size: $L_x = 2\ fm$, $L_y = 15.0\ fm$ and $L_z = 24\ fm$. Space grids are also introduced: $\Delta x = 2\ fm$, $\Delta y = 2.5\ fm$, $\Delta z = 1\ fm$. Evolution of meson particle densities is shown in Fig. 13, starting from $3\ fm/c$ (when the maximum density is approximately reached). At both energies the model predicts approximatelly equal maxima: $\sim 3 - 3.5$ mesons per fm^3, which can be reached after time $t_{cm} \sim 3\ fm/c$, but at $RHIC$ energy the meson density decreases much slower than at $Sp\bar{p}S$ energy. After reaching the maxima meson densities fall to ~ 1 meson per fm^3 for $\sim 3\ fm/c$ at $Sp\bar{p}S$ energy and for $\sim 6\ fm/c$ at $RHIC$ energy respectively.

At ultra–relativistic (especially at $RHIC$) energies, where the produced mesons are concentrated along the light cones, a more suitable evolution parameter is the proper time $\tau = \sqrt{t_{cm}^2 - z_{cm}^2}$, where t_{cm} and z_{cm} are the center of mass time and longitudinal coordinate of the produced hadron. Using Bjorken's formula ([40]) for the meson density:

$$\rho_m = 1/\tau A_{trans} dN/d\eta, \tag{12}$$

where A_{trans} is the Au transverse area, N is the number of produced mesons, and η is the space–time meson rapidity, we can calculate the τ evolution of the meson (and also energy) density by specifying the transverse mass $m_t \approx 0.5\ GeV$. The calculated meson density evolution at both energies looks similar. It reaches a sharp maximum: ~ 3.7 mesons per fm^3 at $\tau \sim 2.0\ fm/c$ and ~ 4 mesons per fm^3 at $\tau \sim 2.5\ fm/c$, at $Sp\bar{p}S$ and $RHIC$ respectively. After the maxima, the meson densities decrease quickly, following a longitudinal $(1/\tau)$ expansion.

The existence during $5 - 7\ fm/c$ of a very dense meson matter is an interesting phenomenon that might deserve intensive studies.

6 Conclusions

The Monte Carlo Parton String Model which intends for simulation of multiparticle production in NN, NA and AA collisions at high energies is described. Comparison to some available experimental data shows that the model works reasonably well and can be useful to study massive ion collisions, as a first approximation.

To make a qualitative analysis we have calculated the mean numbers of both light flavour and charmed hadrons produced in pp, pA, and minimum bias and central $AuAu$ collisions at energies $E_{cm} = 19.4$ and $E_{cm} = 200\ AGeV$. At both energies and for the mentioned colliding systems rapidity distributions for charged, negative and charmed hadrons, negative particle multiplicity distributions, net proton rapidity distributions and meson density evolution have been presented.

We should stress that our simplified model cannot pretend to produce detailed quantitative predictions. First, no hadronic final state rescatterings have been included, which should be important for a more detailed description of nuclear collisions. As we have seen, the meson density can reach ten times the normal nuclear density, so hadron interactions might be crucial for a correct hadron gas evolution, approaching to the mechanical and/or chemical equilibrium, and change significantly the hadron momentum distributions or the hadron content. Second, an independent string formation and decay picture has been used as a basis for particle production. With a number of strings growing as energy and atomic number of the colliding particles get larger, one should expect interaction between the strings and their fusion. Some attempts to include this phenomenon has been published in Ref. [8].

An attempt to include hard perturbative parton scattering and gluon radiation has been made. Hard parton scattering is essential to reproduce the transverse momentum distributions for $p_t > 2\ GeV/c$, and its effect increases with energy. It could also modify heavy flavour production, and has a time scale different from the one in soft interactions (hard interactions could happen at an earlier stage of the reaction, changing the evolution of the colliding system).

In literature some studies of multiple particle production at high energies have been published similar to our approach (a DPM Monte Carlo model ([26]), and an analitical approach ([18])). In Ref. [26] predictions are given for the rapidity and transverse momentum distributions and the minijet component of the hadronic energy density for energies up to $E_{cm} = 6300\ AGeV$. In Ref. [18] the multiplicities and the spectra of various produced particles (including charm) are studied at $E_{cm} = 200\ AGeV$. The main difference of our treatment is in that we consider both hadrons and nuclei on the same footing, introducing partonic wave functions for them. In this unified approach hadronic and nuclear interactions are treated in a similar manner, which is a serious advantage when some sort of interaction between colour strings is introduced (like in Ref. [8]). As for concrete results, our predictions are consistent with those of Refs. [26, 18], except for some specific observables: e. g. we predict $5-7$ times more charmed $D/\bar{D}$ mesons in $AuAu$ collisions at $RHIC$ energy than in Ref. [18].

7 Acknowledgements

The authors are grateful to the Alexander von Humboldt Foundation, and the CICYT of Spain for financial support.

References

[1] Proceedings of the *Quark Matter '91*, Nucl. Phys. **A525** (1992) 1.

[2] B. Andersson, G. Gustafson and B. Nilsson–Almqvist, Nucl. Phys. **B281** (1987) 289; B. Andersson, G. Gustafson and Hong Pi, Z. Phys. **C57** (1993) 485.

[3] H. Sorge, H. Stöcker and W. Greiner, Nucl. Phys. **A498** (1989) 567c; H. Sorge, A. von Keitz, R. Matiello, H. Stöcker and W. Greiner, Phys. Lett. **B243** (1990) 7; A. von Keitz, H. Sorge, H. Stöcker and W. Greiner, Nucl. Phys. **A527** (1991) 601.

[4] K. Werner, J. Hufner, M. Kutschera and O. Nachtmann, Z. Phys **C37** (1987) 57; K. Werner, Phys. Lett. **B219** (1989) 111.

[5] H.–J. Möhring, A. Capella, J. Ranft, J. Tran Thahn Van and C. Merino, Nucl. Phys. **A525** (1991) 493c.

[6] N. S. Amelin, K. K. Gudima and V. D. Toneev, *The Nuclear Equation of State*, Part B, Ed. W. Greiner and H. Stöcker, NATO ASI Series **A216**, Plenum 1989, p. 473; N. S. Amelin, L. P. Csernai, K. K. Gudima, V. D. Toneev and S. Yu. Sivoklokov, Phys. Rev. **D47** (1993) 1413.

[7] J. Bartke *et al.*, Z. Phys. **C48** (1990) 191; R. Stock *et al.*, Nucl. Phys. **A525** (1991) 221c.

[8] N. S. Amelin, M. A. Braun and C. Pajares, Phys. Lett. **B306** (1993) 312; Santiago preprint US–FT/92–18 (submitted to Z. Phys. C); Proceedings of the *XXII International Symposium on Multiparticle Dynamics*, Santiago de Compostela, July 1992 , Ed. C. Pajares, World Scientific 1993, p. 482.

[9] L. V. Gribov, E. M. Levin and M. G. Ryskin, Phys. Rep. **100** (1983) 1.

[10] V. A. Abramovsky, E. V. Gedalin, E. G. Gurvich and O. V. Kancheli, Sov. J. Nucl. Phys. **53** (1991) 271.

[11] A. Capella, U. P. Sukhatme, C.–I. Tan and J. Tran Thanh Van, Phys. Lett. **B81** (1979) 68; Phys. Rep. **236** (1994) 225.

[12] A. B. Kaidalov, Nucl. Phys. **A525** (1991) 39c; A. B. Kaidalov and O. I. Piskunova, Z. Phys. **C30** (1985) 145.

[13] X. Artru and G. Mennessier, Nucl. Phys. **B70** (1974) 93; X. Artru, Phys. Rep. **97** (1983) 147.

[14] R. D. Field and R. P. Feynman, Nucl. Phys. **B136** (1978) 1.

[15] C. De Marzo *et al.*, Phys. Rev. **D26** (1982) 1019.

[16] T. Akesson *et al.*, CERN preprint CERN–EP 111 (1989).

[17] G. I. Lykasov and M. N. Sergeenko, Z. Phys. **C56** (1992) 697.

[18] Yu. M. Shabelskii, Sov. J. Nucl. Phys. **55** (1992) 1399; Z. Phys. **C47** (1993) 409.

[19] M. Aguilar-Benítez *et al.*, Phys. Lett. **B201** (1988) 176.

[20] R. E. Ansorge *et al.*, Z. Phys. **C43** (1989) 357.

[21] G. J. Alner *et al.*, Z. Phys. **C33** (1986) 1.

[22] A. Bamberger *et al.*, Z. Phys. **C38** (1988) 89; C. Albajar *et al.*, Nucl. Phys. **B335** (1990) 261; F. Abe *et al.*, Phys. Rev. Lett. **61** (1988) 1819.

[23] R. E. Ansorge *et al.*, Z. Phys. **C41** (1988) 179.

[24] B. Andersson, G. Gustafson and B. Söderberg, Nucl. Phys. **B264** (1986) 29.

[25] T. Sjöstrand and M. van Zijl, Phys. Rev. **D36** (1987) 2019.

[26] I. Kawrakov, H.-J. Möhring and J. Ranft, Leipzig preprint UL-HEP-92-11.

[27] X.-N. Wang and M. Gyulassy, Phys. Rev. **D45** (1992) 844.

[28] N. S. Amelin, E. F. Staubo and L. P. Csernai, Phys. Rev. **D46** (1992) 4873.

[29] E. Eichten, I. Hinchliffe, K. Lane and C. Quigg, Rev. Mod. Phys. **56** (1984) 579.

[30] T. Sjöstrand, Comput. Phys. Commun. **39** (1986) 347; CERN preprint CERN-TH 6488 (1992); T. Sjöstrand and M. Bengtsson, Comput. Phys. Commun. **43** (1987) 367.

[31] B. Andersson, G. Gustafson, L. Lönnblad and U. Pettersson, Z. Phys. **C43** (1989) 625; U. Pettersson, Lund preprint LU TP 88-5; L. Lönnblad, Lund preprint LU TP 89-10.

[32] T. Sjöstrand, Nucl. Phys. **B248** (1984) 469.

[33] B. Müller and X.-N. Wang, Phys. Rev. Lett. **68** (1992) 2437.

[34] P. Lèvai and J. Zimànyi, Phys. Lett. **B304** (1993) 203.

[35] A. De Rújula, E. Fernández and J. J. Gómez-Cadenas, CERN preprint CERN-TH 6452 (1992).

[36] K. Werner, Phys. Lett. **B219** (1989) 111.

[37] B. Andersson, G. Gustafson, G. Ingelman and T. Sjöstrand, Phys. Rep. **97** (1983) 31.

[38] J. A. Casado, Phys. Lett. **B309** (1993) 431.

[39] K. Geiger and B. Müller, Nucl Phys. **B369** (1992) 600.

[40] J. D. Bjorken, Phys. Rev. **D27** (1983) 140.

Table Captions

Table 1: Model prediction for charmed meson production in pp interactions at $E_{cm} = 27.4\ GeV$, compared to experimental data ([19]).

Table 2: Experimental data ([23]) and model predictions on the average number of given particles, in $p\bar{p}$ interactions at $E_{cm} = 200\ GeV$.

Table 3a: Number of events (N_{evt}), particle production cross sections (σ_{prod}), and mean multiplicities of charged particles (n_{ch}), negative particles (n_{neg}), charged pions ($n_{\pi^\pm}$), charged kaons ($n_{K^\pm}$), protons (n_p), neutrons (n_n), antiprotons ($n_{\bar{p}}$) and lambdas (n_Λ), and the difference between the initial nucleon rapidity and the position of the maxima in rapidity net proton distributions ($y_0 - y_{max}$), in pp, pAu, $AuAu$ and central $AuAu$ collisions at $E_{cm} = 19.4\ AGeV$.

Table 3b: The same as Table 3a, at $E_{cm} = 200\ AGeV$.

Table 4: Mean multiplicities of all charmed hadrons (n_{charm}), $D/\bar{D}$ mesons ($n_{D/\bar{D}}$), and maximum rapidity densities of all charmed particles and $D/\bar{D}$ mesons, in pp, pAu, $AuAu$ and central $AuAu$ collisions at $E_{cm} = 200\ AGeV$. The number of simulated events is shown in Table 3b.

Figure Captions

Figure 1: Nucleon inelastic cross sections as a function of energy. Black circles are the result of the calculation. Open symbols are the experimental data.

Figure 2: Predictions of the model for the mean number of parton–parton collisions as a function of the impact parameter, in pp interactions, at (from the bottom to the top) $E_{cm} = 19.4$, 200, 1800 and 6300 GeV.

Figure 3: Upper figure: calculated distribution (open circles) of the number of participating projectile nucleons, compared to the VENUS model ([4]) predictions (black circles). Lower figure: distribution in the number of parton–parton collisions. Both figures are for ^{16}OAu collisions at 200 $AGeV$.

Figure 4: Rapidity (left figure) and multiplicity (right figure) distributions of negative particles in pp (circles), pAr (triangles) and pXe (diamonds) collisions. The open points are data ([15]), the black ones are model predictions.

Figure 5: Rapidity (upper figures) and transverse momentum (lower figures) distributions of negative particles (left figures) and protons (right figures) in central SS collisions. The transverse momentum distributions of negative particles and protons are in the rapidity interval $0.8 < y < 2.0$. The open points are data ([7]), the black ones are model predictions.

Figure 6: Inclusive x spectrum of all D mesons produced in pp interactions at $E_{cm} = 27.4$ GeV. Black circles are model predicions, triangles with errors bars are data taken from Ref. [19].

Figure 7: Multiplicity distributions (left figure) for charged particles in different pseudorapidity intervals (from the bottom to the top, $|\eta| < 0.5$ $(*10^{-3})$, $|\eta| < 1.5$ $(*10^{-2})$, $|\eta| < 3.0$ $(*10^{-1})$ and full phase space), and semi-inclusive pseudorapidity distributions (right figure) for different multiplicity bins ($2 \leq n \leq 10$, $12 \leq n \leq 20$, $22 \leq n \leq 30$, $32 \leq n \leq 40$, $42 \leq n \leq 50$ and $52 \leq n$) in non-single diffractive $p\bar{p}$ events at $E_{cm} = 200$ GeV, together with experimental data ([20, 21]). Full lines are model predictions, black symbols are experimental data.

Figure 8: Transverse momentum distributions of charged particles in the rapidity interval $2 < y < 4$ in pp collisions at $E_{cm} = 19.4$ GeV (left figure). Invariant inclusive cross sections of charged particles in the pseudorapidity region $| \eta | \leq 2.5$ in $p\bar{p}$ collisions at $E_{cm} = 200$ GeV (right figure). Black points are model predictions, open points are experimental data ([22]).

Figure 9: Pseudorapidity distributions (left figure) and invariant inclusive cross sections (right figure) of charged particles in $p\bar{p}$ collisions at (from the bottom to the top) $E_{cm} = 200$ GeV and $E_{cm} = 1800$ GeV. Black points are model predictions, open points are data ([21, 22]). Both the calculations and experimental data ([22]) in the invariant inclusive cross sections are obtained in the pseudorapidity region $| \eta | \leq 2.5$ and $| \eta | \leq 1$ respectively.

Figure 10: Model predictions for rapidity distributions of charged (*a),c)*) and negative (*b),d)*) particles produced in (from the bottom to the top) pp, pAu, $AuAu$ and central $AuAu$ collisions at $E_{cm} = 19.4$ $AGeV$ (*a),b)*) and 200 $AGeV$ (*c),d)*).

Figure 11: Model predictions of negative particle multiplicity distributions in the whole rapidity interval in pp and pAu (*a),c)*) collisions, and in $AuAu$ and central

$AuAu$ collisions (b),d)), at $E_{cm} = 19.4$ $AGeV$ (a),b)) and 200 $AGeV$ (c),d)).

Figure 12: Space-time picture of meson formation in central $AuAu$ collisions at $E_{cm} = 19.4$ $AGeV$ (left figure) and 200 $AGeV$ (right figure).

Figure 13: Meson density evolution in central $AuAu$ collisions. Upper figures correspond to $E_{cm} = 19.4$ $AGeV$, and have been calculated at center of mass (of the colliding nuclei) time $t_{cm} = 3$ fm/c, $t_{cm} = 6$ fm/c and $t_{cm} = 9$ fm/c. Lower figures correspond to $E_{cm} = 200$ $AGeV$, and have been calculated at $t_{cm} = 3$ fm/c, $t_{cm} = 6$ fm/c and $t_{cm} = 9$ fm/c.

Table 1

Meson	Exp. cross section (μb)	Mod. cross section (μb)	Mean multiplicity
D^+	5.7 ± 1.0	10.35	0.00035
D^-	6.2 ± 1.0	12.48	0.00041
D^0	10.5 ± 1.7	10.35	0.00034
D^0	7.9 ± 1.5	19.17	0.00063

Table 2

Hadron multiplicity	Exp.	Model
$n_{ch}(-3.5 < \eta < 3.5)$	17.6 ± 0.2	16.95
$n_{K^0_s}(-3.5 < y < 3.5)$	0.71 ± 0.08	0.78
$n_{K^\pm}(-3.5 < \eta < 3.5)$	1.15 ± 0.13	1.50
$n_{n+\bar{n}}(-0.5 < y < 0.5)$	0.07 ± 0.03	0.12
$n_{p+\bar{p}}(-3.5 < \eta < 3.5)$	0.6 ± 0.3	0.55
$n_{\Lambda+\bar{\Lambda}+\Sigma^0+\bar{\Sigma^0}}(-2.0 < y < 2.0)$	0.26 ± 0.08	0.25
$n_{\Lambda+\bar{\Lambda}+\Sigma^0+\bar{\Sigma^0}}(-3.5 < \eta < 3.5)$	0.31 ± 0.09	0.29
$n_{\Sigma^\pm+\bar{\Sigma}^\pm}(-3.5 < \eta < 3.5)$	0.16 ± 0.06	0.096
$n_{\Xi^-+\bar{\Xi}^-}(-3.0 < y < 3.0)$	0.03 ± 0.03	0.028
$n_{\Xi^-+\bar{\Xi}^-}(-3.5 < \eta < 3.5)$	0.03 ± 0.03	0.024
$n_{\pi^\pm}(-3.5 < y < 3.5)$	15.9 ± 0.4	15.27

Table 3a

Reaction	pp	pAu	AuAu	$AuAu_c$
N_{evt}	40000	14000	2000	200
$\sigma_{prod}(\ mb)$	28.58	1642.7	6573.2	
n_{ch}	8.75	17.35	535.66	2263.3
n_{neg}	3.26	7.84	252.2	1066.4
$n_{\pi^\pm}$	6.67	14.34	454.1	1923.1
$n_{K^\pm}$	0.63	1.16	39.02	168.35
n_p	1.26	1.67	38.50	156.46
n_n	0.69	1.68	45.74	180.02
$n_{\bar{p}}$	0.058	0.084	1.740	6.860
n_Λ	0.157	0.247	5.544	21.64
$y_0 - y_{max}$	0.92	2.32		1.74

Table 3b

Reaction	pp	pAu	AuAu	$AuAu_c$
N_{evt}	20000	7000	1000	100
$\sigma_{prod}(\ mb)$	43.56	1776.8	6810.9	
n_{ch}	19.62	53.11	1719.7	7575.7
n_{neg}	8.83	25.66	843.40	3717.3
$n_{\pi^\pm}$	15.65	44.82	1470.7	6492.5
$n_{K^\pm}$	2.00	4.61	153.83	678.84
n_p	1.54	2.45	58.99	247.25
n_n	0.93	2.62	66.57	271.38
$n_{\bar{p}}$	0.331	0.691	20.99	91.840
n_Λ	0.340	0.714	18.21	74.89
$y_0 - y_{max}$	1.18	2.78		2.08

Table 4

Reaction	pp	pAu	AuAu	$AuAu_c$
n_{charm}	0.0231	0.0503	1.379	5.92
dn_{charm}/dy	0.0042	0.0097	0.33	1.12
$n_{D/\bar{D}}$	0.0072	0.0167	0.502	2.06
$dn_{D/\bar{D}}/dy$	0.0011	0.0037	0.11	0.41

Fig. 1

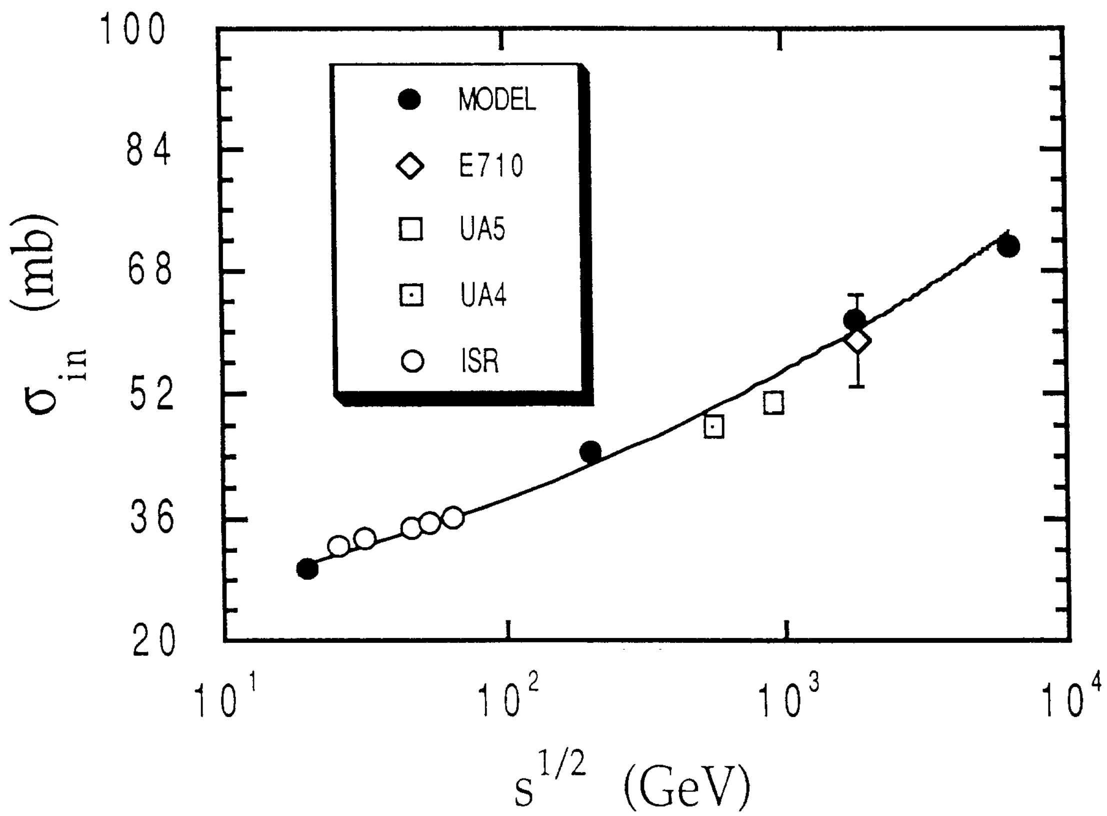

100
84
68
52
36
20
MODEL
E710
UA5
UA4
ISR
σ_{in} (mb)
10^1
10^2
10^3
10^4
$s^{1/2}$ (GeV)

Fig. 2

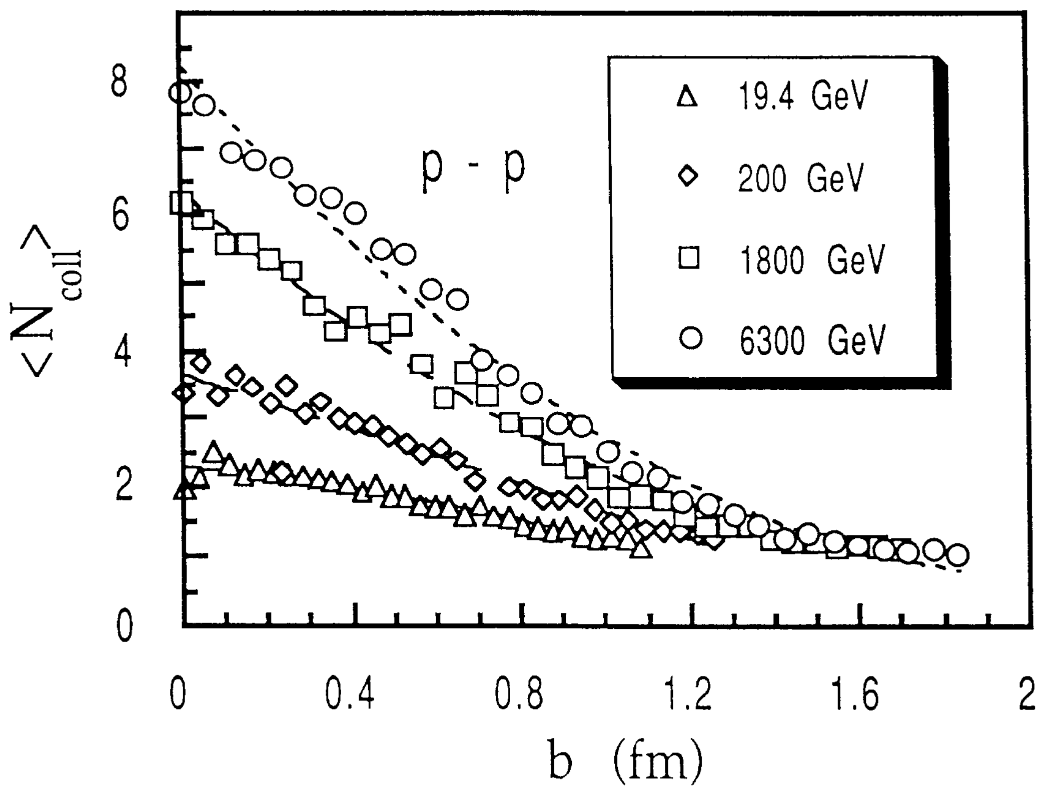
p - p
19.4 GeV
200 GeV
1800 GeV
6300 GeV
<N_coll>
b (fm)
0
2
4
6
8
0
0.4
0.8
1.2
1.6
2

Fig. 3

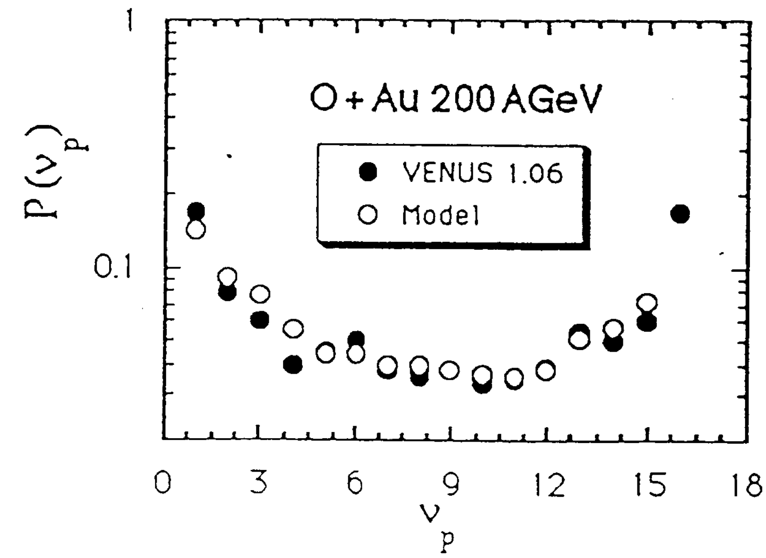

O + Au 200 AGeV
VENUS 1.06
Model
P(ν_p)
ν_p
1
0.1
0
3
6
9
12
15
18

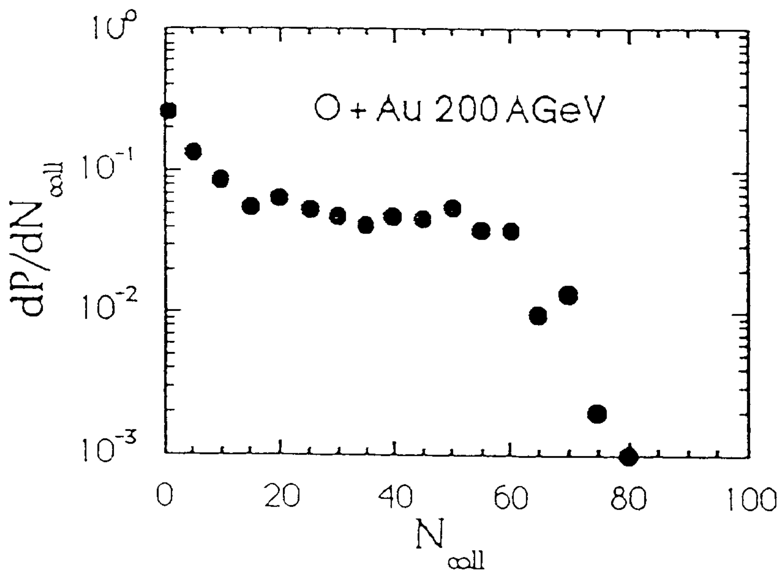

O + Au 200 AGeV
dP/dN_coll
N_coll
10^0
10^-1
10^-2
10^-3
0
20
40
60
80
100

Fig. 4

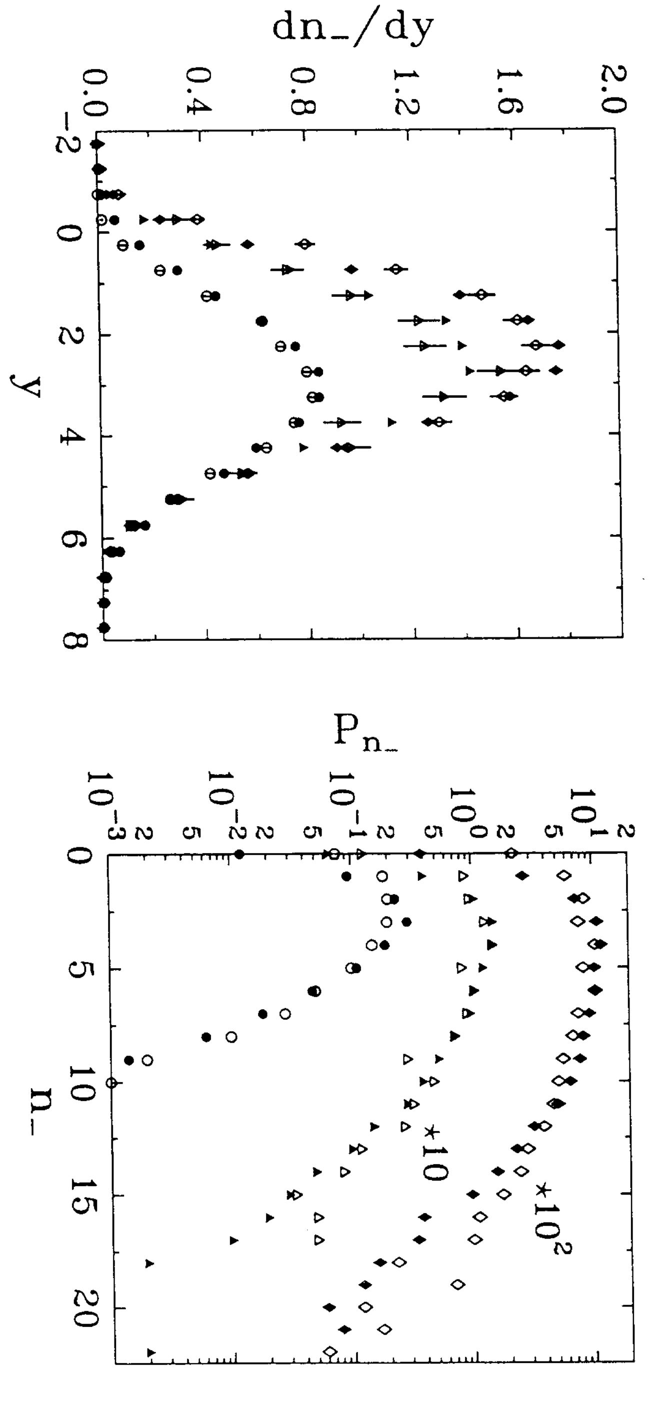

Fig. 5

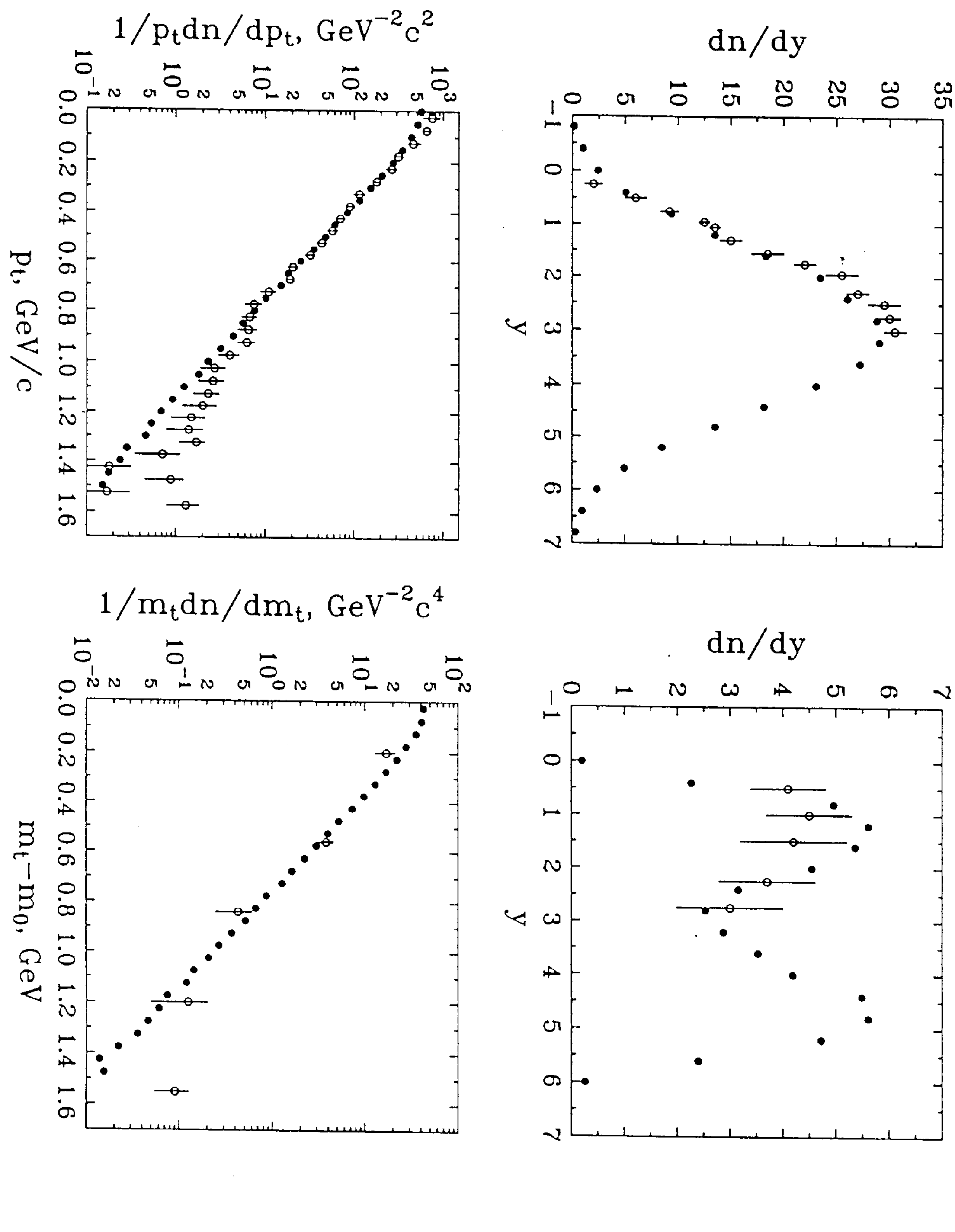
dn/dy
y
dn/dy
y
1/p_t dn/dp_t, GeV^-2 c^2
p_t, GeV/c
1/m_t dn/dm_t, GeV^-2 c^4
m_t-m_0, GeV

Fig. 6

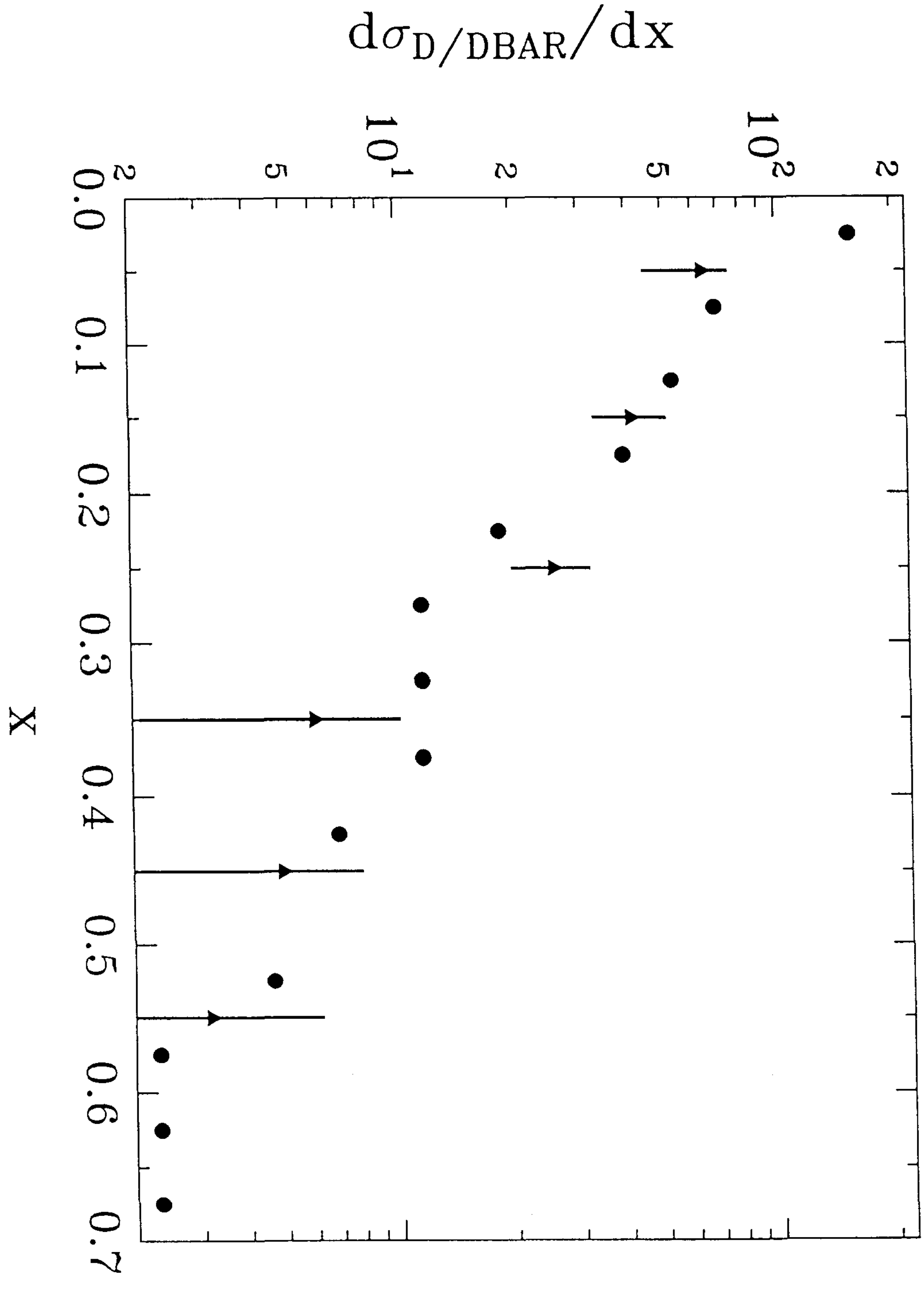

Fig. 7

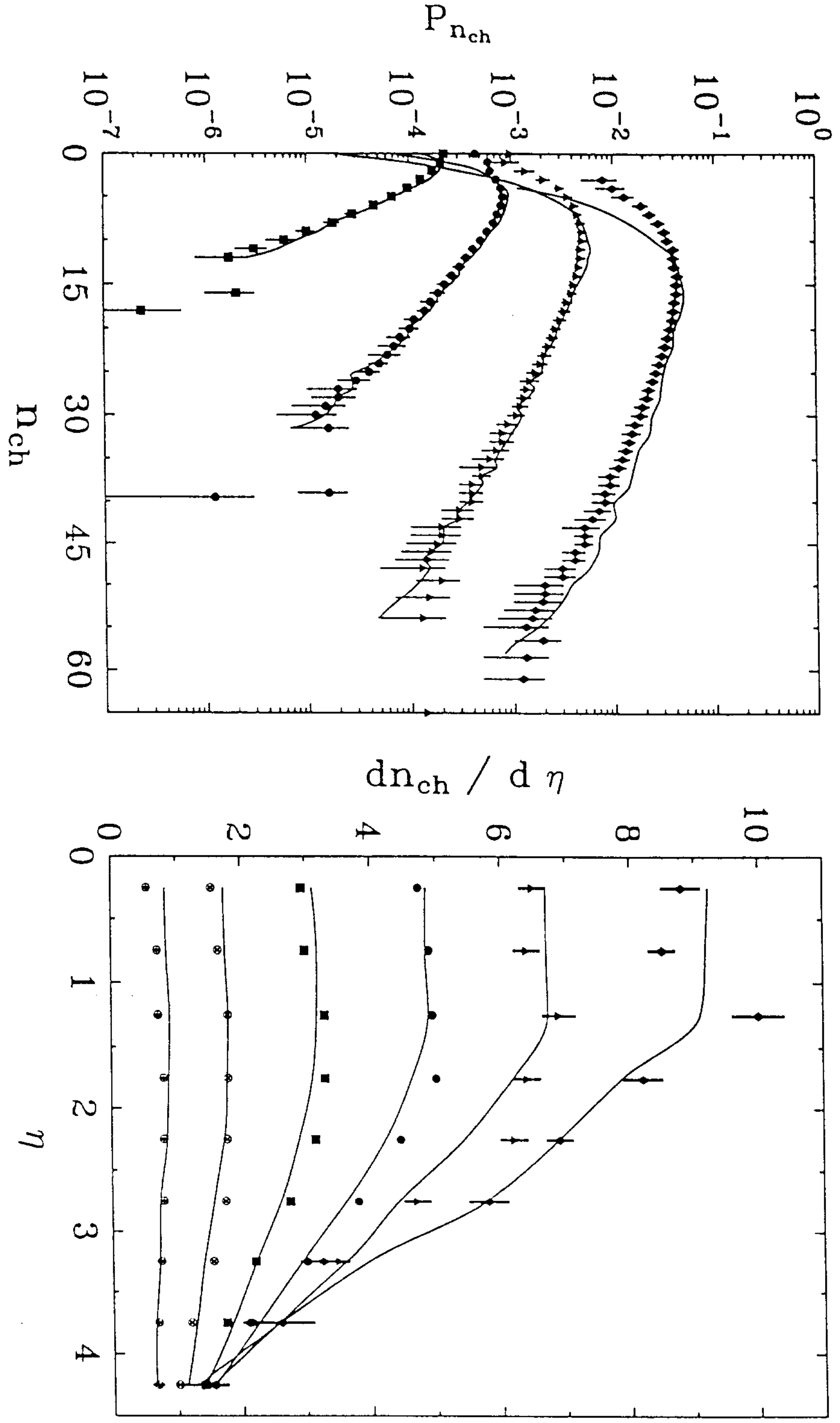

Fig. 8

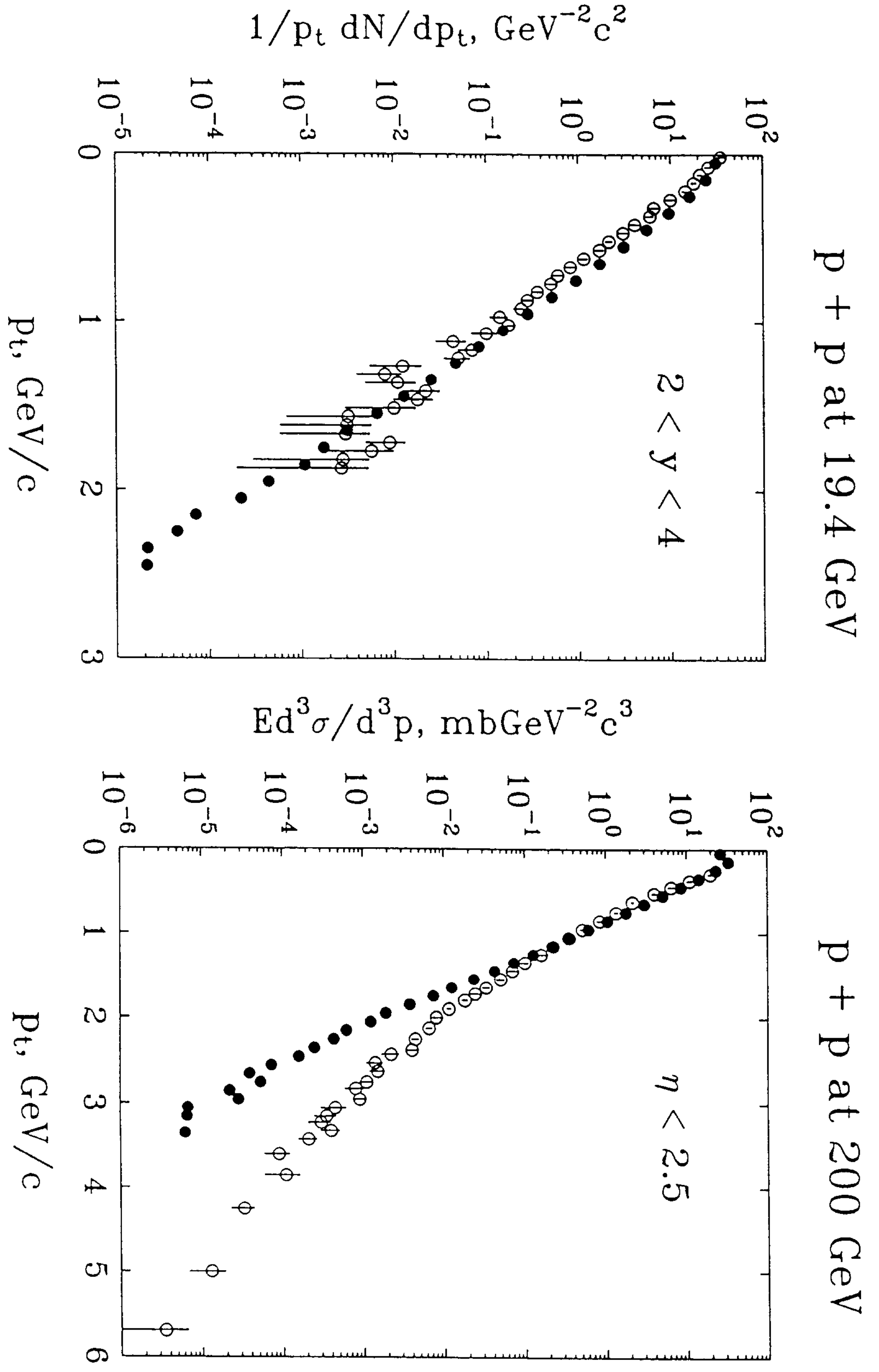
p + p at 19.4 GeV
2 < y < 4
1/p$_t$ dN/dp$_t$, GeV^{-2}c^2
Pt, GeV/c
p + p at 200 GeV
η < 2.5
Ed^{3}σ/d^{3}p, mbGeV^{-2}c^3
Pt, GeV/c

Fig. 9

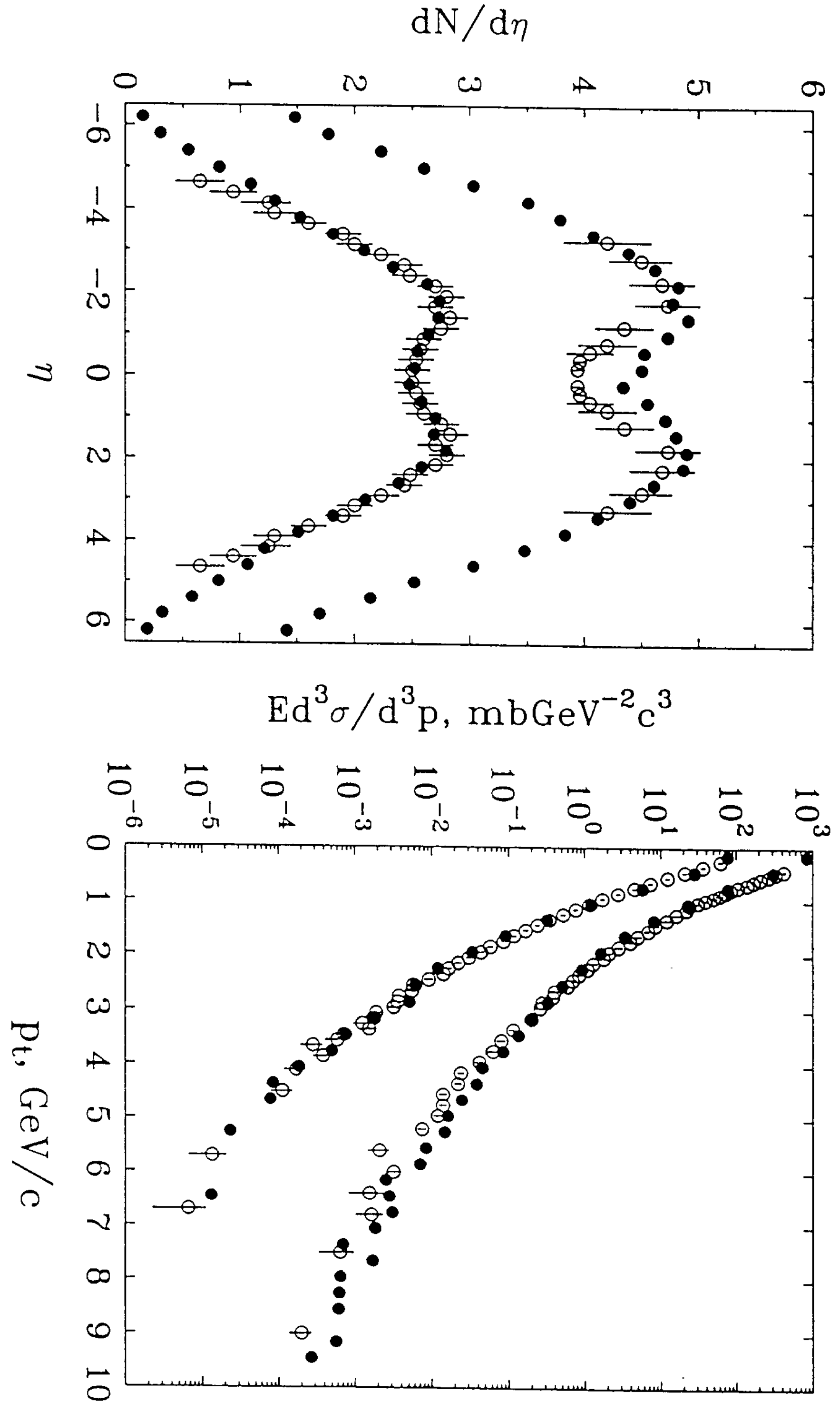

Fig. 10

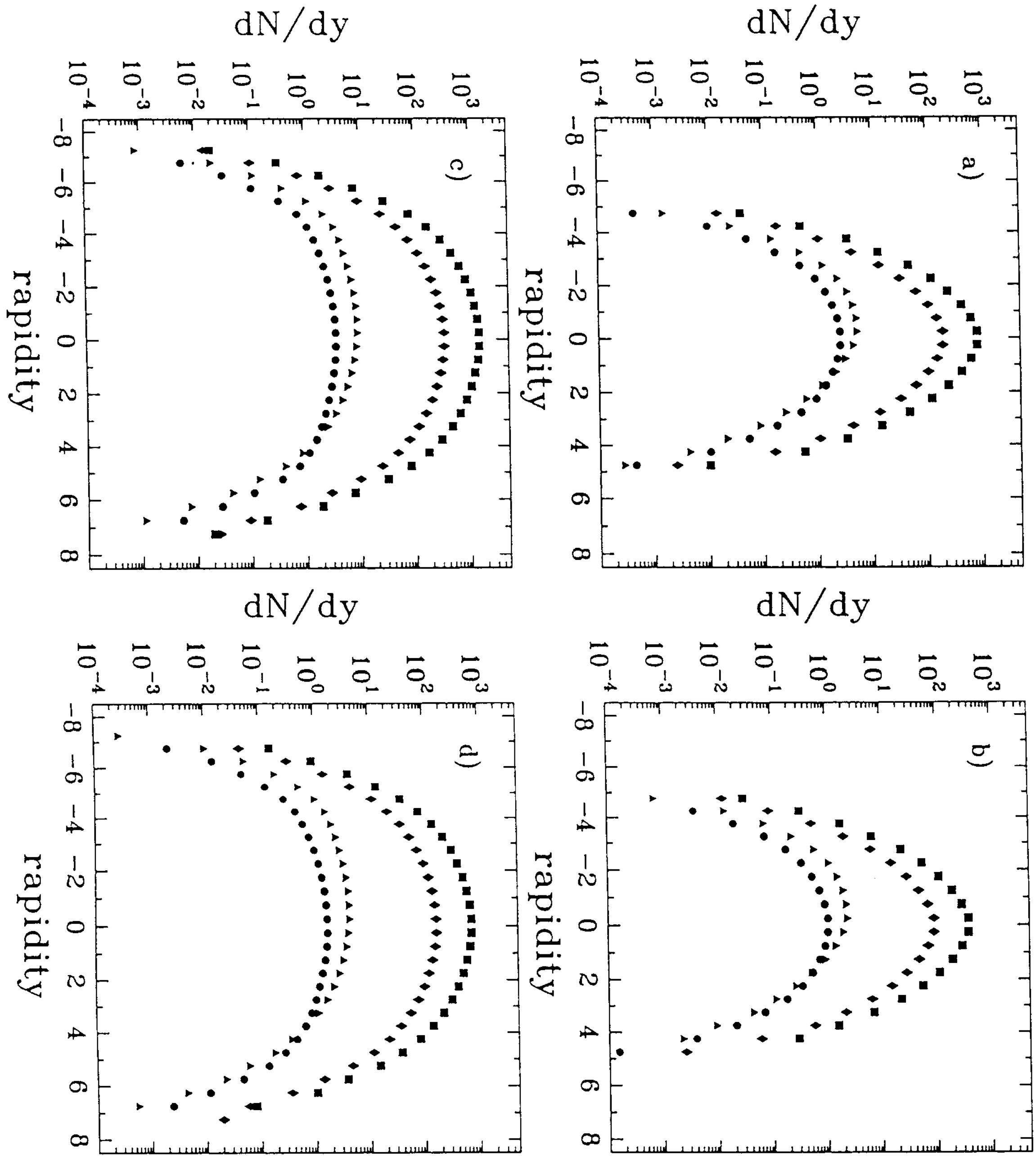

Fig. 11

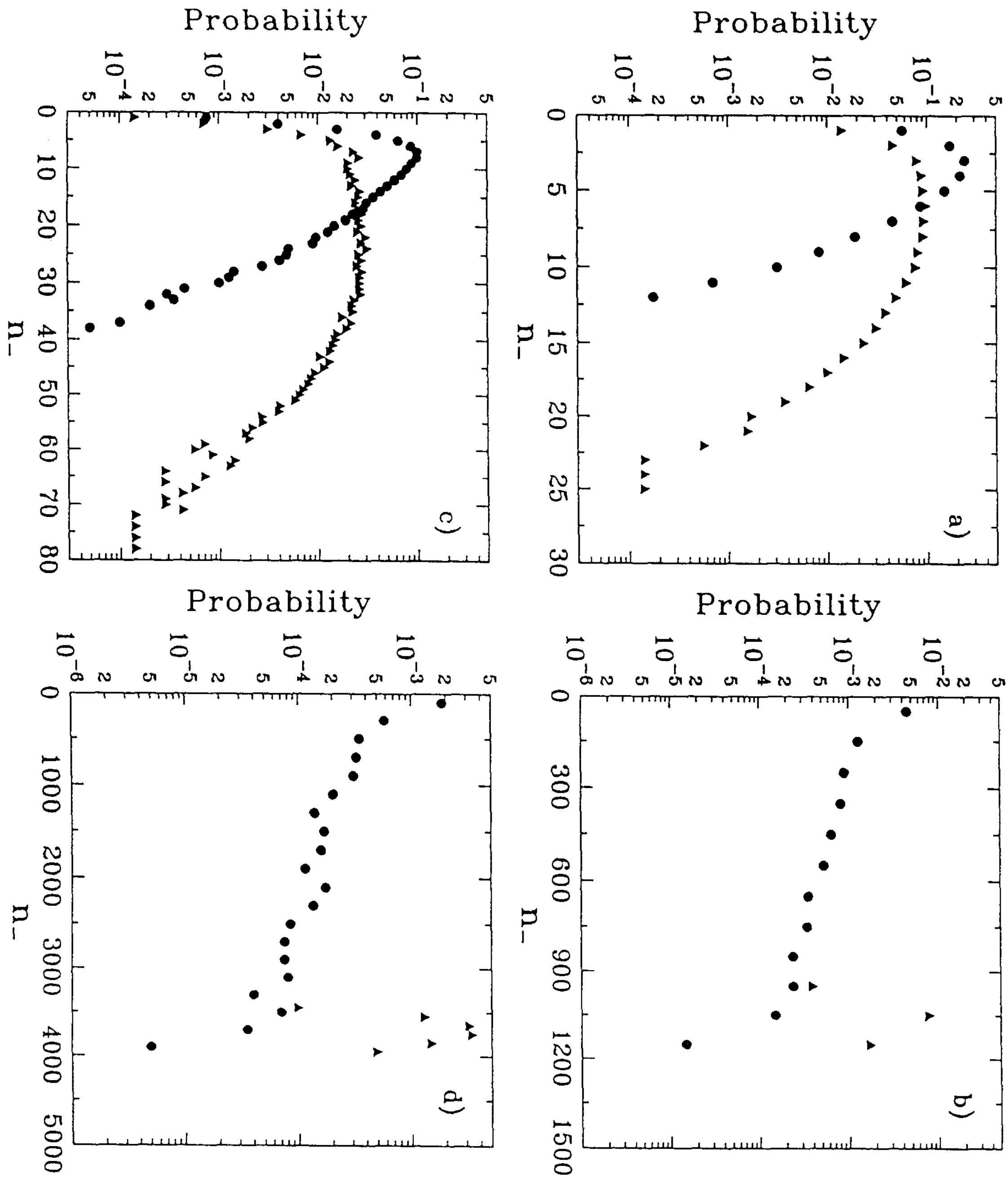

Fig. 12

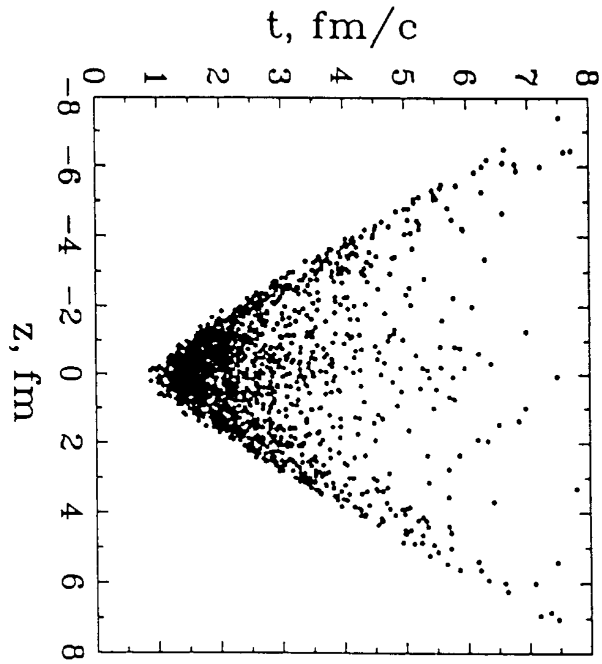

t, fm/c
0
1
2
3
4
5
6
7
8
−8
−6
−4
−2
0
2
4
6
8
z, fm

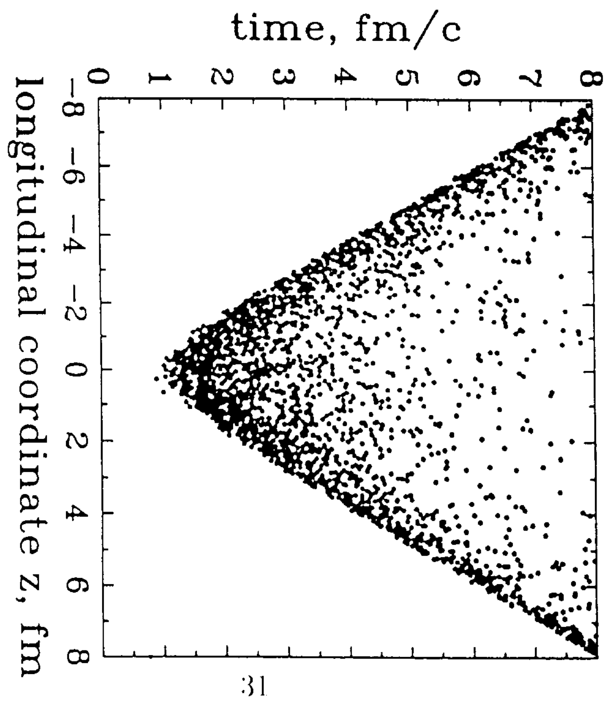

time, fm/c
0
1
2
3
4
5
6
7
8
−8
−6
−4
−2
0
2
4
6
8
longitudinal coordinate z, fm

Fig. 13